İSTANBUL TECHNICAL UNIVERSITY ★ INSTITUTE OF SCIENCE AND TECHNOLOGY

VORTICES CHARACTERIZATION IN A CAVITY FLOW AT LOW SPEED

M.Sc. Thesis by

Elif Özsoy, B.Sc.

Department : Aeronautical Engineering

Programme: Aeronautical Engineering

JANUARY 2003

ACKNOWLEDGEMENT

First of all, I am indebted to Prof.Dr. M. Zeki Erim for his generous support and constructive advises. He has never lost hope in me and for this I am grateful to him.

I would like to thank my supervisor Prof.Dr. Adil Yukselen for his guidance and recommendations during this thesis.

I also would like to thank my supervisor at von Karman Institute M. Riethmuller who has supported me enormously during this thesis. I would like to express my gratitude to my advisor, Dr. Patrick Rambaud for his comments and creative ideas. From the beginning, he had given me a lot of opportunities to broaden my horizons. I want to thank him for his confidence in me. I also sincerely thank to the VKI. Family.

I would like to thank my friends, Sofia, Dilek, Patrick, Murat, Bahadir, Tayfun, Nejat Ulas….You were always by my side.

Lastly, I would like to dedicate my thesis to my parents who give the greatest support and encouragement to me.

December, 2002 Elif Özsoy

CONTENTS

LIST OF TABLES

LIST OF FIGURES

Page No

LIST OF SYMBOLS

$\mathbf{Re_h}$	**:** Reynolds number based on cavity step height
h	**:** Step height
L	**:** Cavity length
$\mathbf{U_0}$	**:** Uniform free stream velocity
δ	**:** Boundary layer thickness for incoming flow
θ	**:** Momentum thickness for incoming flow
$\mathbf{\delta^*}$	**:** Displacement thickness for incoming flow
ω	**:** Vorticity
Γ	**:** Circulation of vortex
S, Ω	**:** Decomposition parts of velocity gradient tensor
E	**:** Enstrophy of the vortex
λ	**:** Lamda field (eigenvalue of the velocity gradient tensor)
u', v'	**:** Turbulence intensities
$\mathbf{Re_\theta}$	**:** Reynolds number based on momentum thickness

DÜŞÜK HIZLI KAVİTE İÇİ AKIŞTA DÖNGÜ DAVRANIŞLARININ İNCELENMESİ

ÖZET

Türbülanslı akışların ayrılması ve tekrar yüzeye yapışması gerek iç gerekse dış akış içeren çeşitli mühendislik uygulamalarında karşımıza çıkmaktadır. Bu uygulamalara örnek olarak yayıcılar, yanma odası akışı, ani genişlemeye sahip kanallar ve bina ve kanat üzerindeki akışlar gösterilebilir. Ayrılmalı akışların en iyi temsil edildiği geometrilerden biri kavite akışıdır. Kavite akışının karmaşıklığı asal olarak akış ayrılma bölgesinde ortaya çıkan ve akışla beraber taşınan döngülerden kaynaklanmaktadır.

Bu tez kavite akışı içerisindeki döngülerin davranışlarını istatistiksel olarak incelemek amacıyla yapılmıştır. Bu yüzden geniş ve güvenilir bir veri tabanı oluşturulmaya çalışılmıştır.

Deneysel içerikli bu çalışma düşük hızlı bir hava tünelinde parçacık izleme yöntemi (PIV) kullanılarak gerçekleştirilmiştir. Deneyler kavite uzunluğunun derinliğine oranı dört olan dikdörtgen kavite geometrisi (açık ve sığ) için yapılmıştır. Kavitenin derinliği ve gelen akımın hızı esas alınarak hesaplanmış üç farklı Reynolds sayısı ile çalışılmıştır. Akışın giriş koşulları sıcak tel anemometrisi kullanılarak belirlenmiştir ve laminer rejime uyduğu görülmüştür. Döngülerin PIV ölçümleri ile elde edilen anlık hız alanlarından çıkartılması *wavelet analiz* yöntemi ile sağlanmıştır.

Sonuçlar, ortalama akış büyüklükleri ve aynı zamanda istatistiksel döngü karaktersitikleri cinsinden verilmiştir.

İncelenen kavite akışında akım yapışması gözlenmediğinden akışın "açık tip" kavite akışı olduğuna karar verildi. Ayrıca akışın birbirine ters yönde dönen iki döngü ile temsil edildiği tespit edildi. Reynolds sayısı arttırıldığında bu her iki döngünün de akışın gelmekte olduğu yöne doğru hareket ettikleri ve aynı zamanda kavitenin arka basamağında konumlanan döngünün boyutunun büyüdüğü görüldü. Bu büyümenin hızlanmakta olan akışın döngülere verdiği enerjiden kaynaklandığı sonucuna varıldı.

Yerleri ve boyutları wavelet analizi ile belirlenmiş döngülerin genel dağılımına bakıldığında bunların kavitenin ön basamağından çıkan bir jet akışına benzediği görüldü. Döngülerin iki ana üretim kaynağı olduğu tespit edildi. Saat yönünde dönen döngülerin ayrılmanın meydana geldiği kayma tabakası içerisinde oluştuğu ve yollarına kavitenin arka basamağında oluşan ana döngü aracılığıyla devam ettikleri belirlendi. Saatin ters yönünde dönen döngülerin ise kavitenin arka duvarında gelişen sınır tabaka etkisiyle oluştuğu ve genellikle kavitenin ön tarafında konumlandığı görüldü. Döngülerin boyutlarının ise yaklaşmakta olan sınır tabaka kalınlığı ile ilişkili olduğu ve Reynolds sayısı arttırıldığında azaldığı tespit edildi.

VORTICES CHARACTERIZATION IN A CAVITY FLOW AT LOW SPEED

SUMMARY

Separation and reattachment of turbulent flows may be encountered in many practical engineering applications both in internal flows such as diffusers, combustors and channels with sudden expansion and external flows like those around airfoils and buildings. Among the flow geometries used to study separated flows, the cavity flow is one of the most representative ones. The complexity of cavity flows arises from the fact that they are mainly characterized by the vortical events imbedded in the separated shear layer and convected downstream of the cavity leading edge.

The present thesis is aimed primarily to understand the nature of the vortex behavior in a cavity flow through the analysis of statistical data. The second aim is to create a wide and reliable database for such a complicated flow and to try to answer questions related to the creation of vortices, their dimensions, energy contents and locations.

This study which is of experimental nature was performed in a subsonic wind tunnel using particle image velocimetry (PIV). The tests were made on a rectangular cavity with length to the depth ratio of 4 (shallow and open type). Three different Reynolds numbers, based on step height and uniform velocity, were examined (Re=4000,9000,13000). The flow conditions of the upstream boundary layer was investigated using hot-wire anemometry and was found to be laminar. The vortices have been identified by using a wavelet analysis technique applied to instantaneous velocity fields obtained by PIV.

The results are given in terms of conventional quantities and also in terms of vortex characteristics (such as presence of vortices, their trajectories, sizes and circulations).

The results showed that the investigated flow was belonging to an open type and was mainly characterized by two large circulating bubbles turning in opposite directions. As the Reynolds number increased, the downstream recirculation bubble became larger and its center moved through the leading edge. Consequently, the upstream recirculation decreased in size. The enlargement of the downstream recirculation bubble with increasing free stream velocity was attributed to the increasing energizing effect of the shear layer.

An over view of the positions occupied by the vortices was found similar to a jet configuration attached to the leading edge. Two main areas of vortex production were identified. Clockwise vortices are created inside the shear layer, convected by the trailing recirculation bubble. Anti-clockwise vortices were mainly created by the trailing wall-layer. Their concentration at lower Reynolds number seems to be higher in the leading edge recirculation bubble. It is observed that the size of the vortices is

linked to the size of the incoming boundary layer and this size decreases as the Reynolds number increases.

1 INTRODUCTION

Separation and reattachment of turbulent flows occur in many practical engineering applications, both in internal flows system such as diffusers, combustors and channels with sudden expansion, and in external flows like those around airfoils and buildings.

One application is the internal flow inside the solid rocket motor (ARIANE 5). This booster is made of three segments separated by inhibitors as shown in Fig. 1. When the combustion begins, these inhibitors become an obstacle for flow which experiences an adverse pressure gradient along its flow direction and thus flow separation occurs at the obstacles.

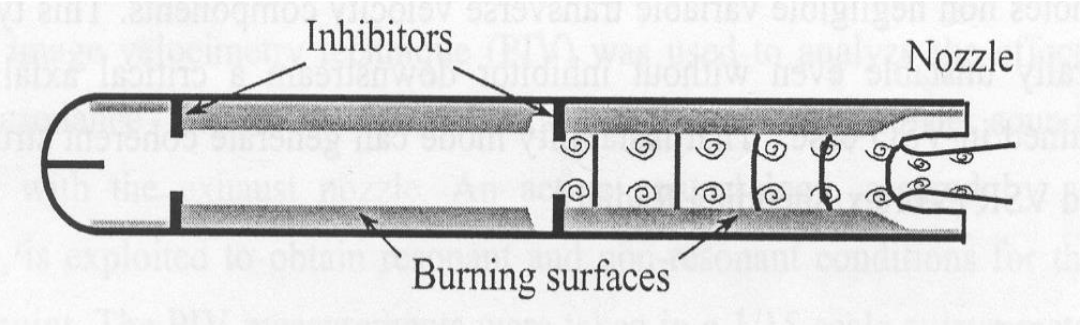

Figure 1.1 An example to cavity flow: internal flow inside solid rocket motor

The flow subsequently reattaches downstream of the inhibitors forming a recirculation bubble between the reattachment zone and the inhibitor itself. The separating shear layer forms vortices downstream of the inhibitor via vortex stretching mechanism. These vortices are shed with certain frequency, which in return can affect the acoustic field i.e., pressure fluctuations within the booster.

Among the flow geometries used for the studies of separated flows, the most frequently selected one is the cavity flow. This study also uses a cavity to simulate the internal flow of a solid rocket motor due to its geometrical simplicity.

Flow past cavities, is an important example of separated flows, which is the most complicated phenomenon in fluid dynamics. Therefore, the flow field around cavities is a good tool for increasing knowledge about flow separation, turbulence and vortex

generation. In addition, this phenomenon has some important applications in industrial aerodynamics, aeronautics and even in hydraulic engineering.

Considering two-dimensional cavity flows, the flow comes from upstream. At the step level separation occurs. The schematic diagram in Fig.1.2 shows a free shear layer emanating from the step. Shear creates vortices, which are transported downstream of the separation point. When these vortices hit the walls of the cavity instabilities occur.

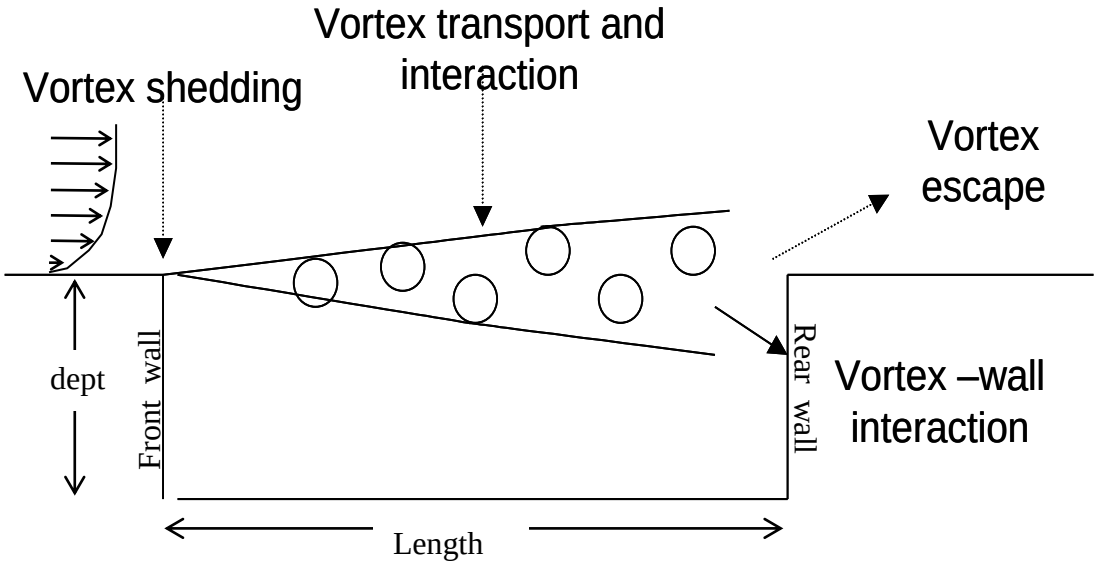

Figure 1.2 Cavity flow nomenclature

These instabilities induce pressure fluctuations occurring at specific frequencies and therefore the entire system when excited may go under resonance, which may eventually destroy the system itself. For low speed cavity flow at rather low values of length/depth ratio, the separated flow either reattaches at the rear wall of the cavity or escapes from the cavity without striking it at all. At the point of reattachment the pressure is higher than the pressure at the proximity of the front wall. Therefore a large reverse flow (captive eddy) establishes itself within the cavity. (Rossiter,(1964))

Cavities have been extensively studied in the past because of their continuous presence in common industrial and military applications. The velocity driven cavity or lid driven cavity has been chosen to be a numerical benchmark (Shankar and Deshpande (2000)). It's experimental counter part is the shear driven cavity. Previous reviews collecting extensive works done in this field have been proposed by

Rockwell (1978) or Komerath et al. (1987) for a non-exhaustive list. Most of the measurements were taken at subsonic, transonic or/and supersonic Mach numbers. Relatively a few numbers of work were done at very low Mach numbers (Tam and Block (1978), Sinha (1981), Gharib and Rosko (1987), Howe (1997) among others). On the theoretical point of view, vortex sheet type model has been introduced by Stuart (1967) and this model is used in linear and non-linear instability studies (Ho and Huerre 1984). Those models were able to describe the possible flapping of the shear layer and it's consequence on the pressure field through the interaction with the trailing edge.

The present work is not directly concerned by vortex sheet type model. But the aim is to extract information about possible vortex events from instantaneous velocity field measurements. Since some decades, although the swirling motion in a cavity has been observed by using smoke visualization techniques, real measurements based on vortex population (size, more probable position) are still missing in this field. For this purpose, in this work the geometrical forms and locations of the vortices are investigated statistically along with their energy content. Our experimental approach is based on high spatial resolution measurement of the cavity flow with the help of particle image velocimetry. This technique allows us to obtain detailed information about two-dimensional instantaneous velocity components of the airflow. Sufficient number of images were collected to obtain a representative mean flow field. Flow structures were detected and located by wavelet analysis.

Following an introduction, the experimental set-up and flow conditions are given in detail in the second chapter. Third chapter is about Vortex identification. In the fourth part, the post-processing is explained shortly. The main section 5 is presenting the experimental results. And in the last chapter, conclusions are presented.

2 EXPERIMENTAL SET-UP

In the following paragraphs detailed descriptions of the experimental conditions are given.

2.1 Wind Tunnel

The experimental investigations were performed in an open circuit, subsonic and vertical wind tunnel. The channel is operated by a suction type blower keeping a low speed velocity in the range of 1 to 20 m/s. The cross sectional dimensions of the test section is 300x100 mm^2 just before the step. A schematic of the test section is depicted in Figure 2.1.

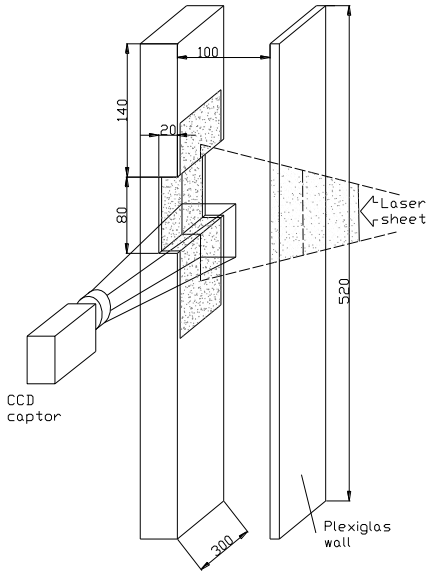

Figure 2.1 Test section of the cavity flow with sketch of the camera and of the laser sheet

The entire measurement campaign was made on a rectangular cavity with a constant step height (h = 20 mm.) and a constant cavity length (L = 80 mm). Therefore the expansion ratio (the ratio of the total height of the test section to the height of the upstream test section) was equal to 1.2 and the aspect ratio (ratio of the span wise test section length to the step height of the cavity) was equal to 15.

2.2 Inlet Conditions

For the cavity flows the investigation of the incoming boundary layer is reported by Sarohia(1977), Karamcheti (1955) as a critical issue to characterize the cavity flow Therefore preliminary hot wire measurements have been done to characterize the incoming flow conditions.

Instantaneous velocities are measured in the incoming boundary layer, at three streamwise locations upstream of the separation edge (i.e. x/h=-0, x/h=-1, x/h=-3) for two different free stream velocities (associated with Re = 4000 & 9000, based on step height), and for several cavity length/height ratio During these measurements, the data were sampled at 3 kHz during 10 seconds at different y/h stations. For all conditions, non-dimensional velocity profiles are plotted in Figure 2.2 (where y is the distance from the surface in vertical direction). The velocity profiles obtained from PIV measurements (just before the separation) for three different velocities are also presented in this figure. A good agreement between these two different techniques is found. These experimental results are compared also with theoretical velocity profiles of laminar and turbulent boundary layers (Schlichting(1968)). Although the results do not coincides with the turbulent boundary layer profile, the agreement with the laminar profile is good.

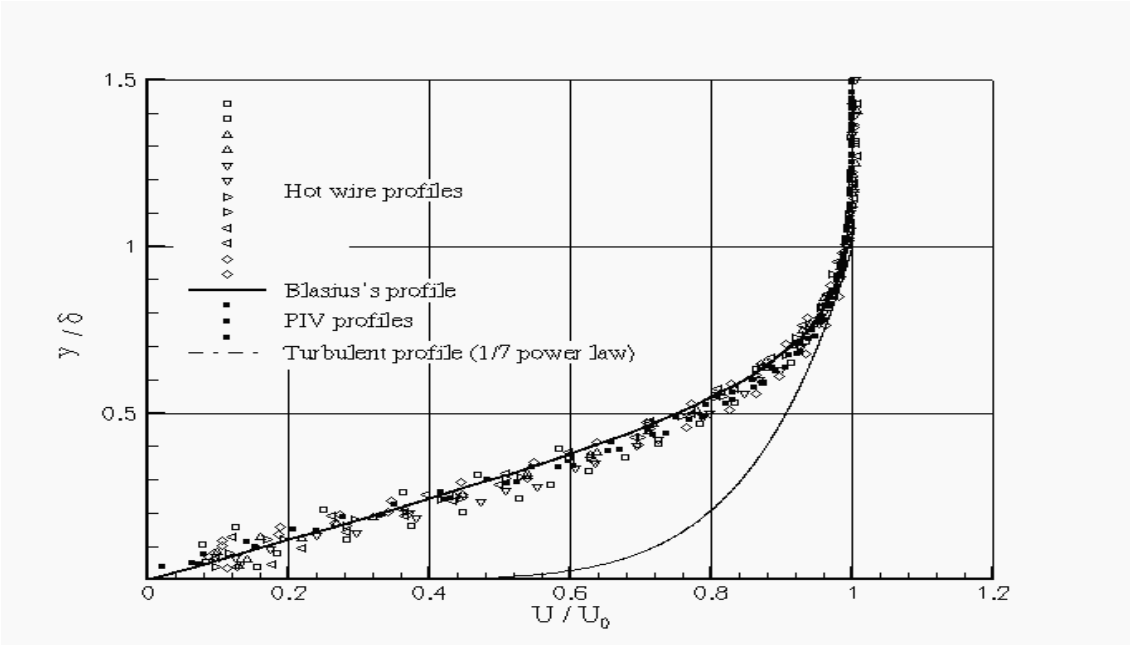

Figure 2.2: Velocity profiles for inlet conditions

Smoke flow visualization has been also employed to obtain qualitative pictures of the cavity (Figure 2.3). In this picture, the laminar state of the incoming flow may be appreciated through the straight path of the smoke following filament like traces.

Figure 2.3: Flow visualization for a free stream velocity of 3 m/s (Re_h=4000)

In Table 2.1 dimensionless parameters as Reynolds number, boundary layer thickness, displacement thickness, momentum thickness are presented to give an idea about the type of incoming boundary layer. Since the ratio between displacement thickness and boundary layer thickness would be about 0.12 for a turbulent boundary layer and 0.32 for a laminar boundary layer over a flat plate (White, (1991)), this table also indicates the incoming boundary layer is a laminar one.

Table 2.1 Dynamical parameters of the incoming boundary layer

	Re_h	δ/h	δ^*/h	θ/h	δ^*/δ
CASE 1	4000	$28.7x10^{-2}$	$9.3x10^{-2}$	$3.5x10^{-2}$	0.32
CASE 2	9000	$22.9x10^{-2}$	$6.9x10^{-2}$	$2.8x10^{-2}$	0.30
CASE 3	13000	$20.7x10^{-2}$	$6.2x10^{-2}$	$2.5x10^{-2}$	0.30

2.3. Technical aspect of PIV measurements

To meet the objectives set for this study, data were obtained with non intrusive velocity measurement technique called particle image velocimetry.(PIV)

Particle Image Velocimetry is based on the measurement of the velocity of tracer particles carried by the fluid. For this purpose, a complete plane of the flow under investigation is illuminated by a narrow light sheet which is spread over the region of

interest. Tracer particles are therefore made visible and images of the illuminated particles are recorded. These recordings contain successive frames of instantaneous images of the whole flow field. And, these data gives the instantaneous velocities of the traces. For further information, reader can consult Raffel et al. (1998) or Scarano (2002) for a review.

In the present study, the laser sheet was generated by a Nd:YAG double pulsed laser. Cylindrical lenses allow the formation of a laser sheet of 0.5 mm thickness. A smoke generator was used to seed the flow with fine oil droplets of 1 μm diameter. A digital CCD cooled camera (PCO Sensicam with a resolution 1280×1024 square pixels) was used to record the successive images at 4.9 Hz with 1280×832 pixels. The pulse separation between two images of the same PIV couple was corresponding to a maximum displacement over the whole field of about 8 pixels (with ΔT=130~40μs). The spatial calibration gave an estimation of 52 μm corresponding to the length of 1 pixel. The PIV measurements are performed in a 67x43 mm^2 field of view. In order to keep a high resolution over the region of interest, the entire measurement domain was splitted in two areas with an overlapping boarder. The first area (called hereafter upstream) was capturing the leading edge of the cavity, the second one (called hereafter downstream) was capturing the trailing edge of the cavity. Those two regions were combined to investigate the whole cavity. It has to be underline that the spatial resolution in both part of the cavity was kept equal and that the time tracking of the vortex was not the scope of our study (velocity fields are uncorrelated in time). The PIV acquisition parameters are collected in Table 2.2.

Table 2.2. PIV acquisition parameters

Acquisition parameters	**case1 (Re_h=4000)**	**case2 (Re_h=9000)**	**case3 (Re_h=13000)**
image size	[1280x832] px^2	[1280x832] px^2	[1280x832] px^2
calibration	~ 5.2 x 10^{-2} m/px	~ 5.2 x 10^{-2} m/px	~ 5.2 x 10^{-2}m/px
pulse separation	130 μs	56μs	37μs
frequency of camera	4.9 Hz	4.9 Hz	4.9 Hz
number of samples	1000 couples/zone	1000 couples/zone	1000 couples/zone

3 IDENTIFICATION AND CHARACTERIZATION OF VORTICES

3.1 About coherent structures

Because turbulence is one of the most complex phenomena in classical physics, the study of coherent structures remains a delicate subject in fluid dynamics, and an 'universal definition' is still missing. Since Kolmogorov's concept, we know that the energy is exchanged from the mean flow to the turbulent flow at the level of the largest scales, and transferred from the largest to the smallest ones, where it is dissipated by viscosity. This concept of energy cascade shows the important role played by these structures : they carry the energy of the turbulence and therefore govern the development of any turbulent flow.

The coherent structures of a particular flow are similar in form but far from identical and they do not appear with precise regularity in either time and space. This lack of regularity is what makes them so difficult to define and describe. A more restrictive definition is given by Hussain (1997): ' a coherent structure is a connected turbulent fluid mass with instantaneously phase-correlated vorticity over its spatial extend '. In any case, coherent structures are three-dimensional and the random nature of turbulence makes their signal-to-noise ratio very low : as a consequence, their eduction from the noisy data is difficult.

The designation of coherent structures remains very general and they can appear under many different figures. In the scope of this research, we are interested in a particular kind of vortices created in a cavity flow. The behavior of the vortex structures can be investigated in 2-D by considering their cross-section in a plane perpendicular to their core. The famous Kelvin-Helmholtz instability causes the shear layer to roll-up into discrete vortices perpendicular to the main flow. Then, several processes have been identified : vortex stretching, pairing, tearing, reconstruction, breakdown … These basic mechanisms are relatively simple when

taken separately, but they become much more complex when they interact, as they do in fully turbulent flow.

3.2 Characteristics of a vortex

It is now important to define what we call a vortex, to find by which quantities it can be characterized, and how it can be modeled. A first topological definition is that 'a vortex exists when instantaneous streamlines mapped onto a plane normal to the vortex core exhibit a roughly circular or spiral pattern, when viewed from a reference frame moving with the vortex core'. In other words, we could say that a vortex is a region where the instantaneous flow is 'turning' uniformly around its center, and which can be convected by a certain velocity.

The characteristic parameters of a vortex are mainly :

- the position of its center (x_0, y_0)
- its velocity distribution ($V = u + v$)
- its convection velocity (u_0, v_0)
- its diameter (D_{vortex})
- its vorticity peak (Ω) and vorticity distribution (ω)
- its circulation (Γ)
- its enstrophy (E)

where $$\omega = \frac{\partial v}{\partial x} - \frac{\partial u}{\partial y} \qquad (3.1)$$

$$\Gamma = \oint_c \vec{V}.d\vec{l} \qquad (3.2)$$

$$E = \iint \omega^2.dxdy \text{ (energy of rotation contained in the vortex)} \qquad (3.3)$$

Different models of vortex have been proposed. Among these different models, the most 'physical' is often said to be the **Oseen vortex**, defined by the following velocity distribution (in polar coordinates r, θ) :

$$\begin{cases} V_\theta = \dfrac{\Gamma_0}{2\pi * r}\left[1 - \exp\left(\dfrac{-r^2}{\sigma^2}\right)\right] \\ V_r = 0 \end{cases}$$

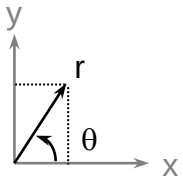

where σ is a characteristic dimension of the vortex.

In figure 3-1, the 2D-pattern of this vortex is shown in (a), while (b) shows the velocity and vorticity distributions along a diameter.

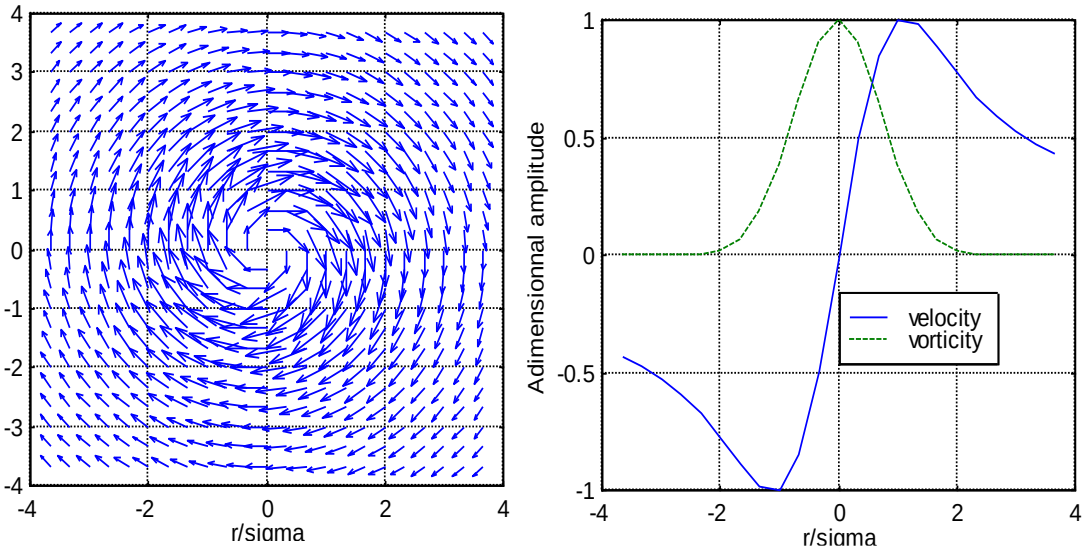

(a) (b)

Figure 3.1 : Illustration of an Oseen vortex (Γ_0=1, σ=1)

(a) flow pattern

(b) velocity and vorticity distributions

3.3. Identification of a vortex

Now that a vortex has been defined and characterized, the aim is to know how to detect it in a flow field. Hussain recalls the different criteria used until now. First of all, we know that the center of a vortex correspond to a local pressure minimum. Unfortunately, a map of pressure is difficult to obtain experimentally, and moreover, a pressure minimum can also exist out of a vortex. The most straightforward criterion used is the presence of the peak of vorticity at the center of the vortex. Indeed, the

vorticity is a Galilean invariant of the velocity, which means that it is not affected by an additional convection velocity. If a vortex present always a peak of vorticity, the contrary is not true in every cases (as for the pressure minimum). In particular, the presence of shear in the flow gives rise to vorticity that does not correspond to a vortex : like in a shear, mixing, or boundary layer. Because this research deals with a flow where the shear layer has a capital importance, it seems necessary to find another criterion.

Another way to identify a vortex, proposed by Hussain, will now be described.

Any tensor can be decomposed in a symmetric and antisymmetric part. When this decomposition is applied to the tensor of the velocity gradients, one obtains the tensors of deformation and rotation respectively : $\nabla U = S + \Omega$

Let's now consider the following tensor $S^2 + \Omega^2$. From the Navier-Stokes equation, it comes that the flow contains a local pressure minimum if this tensor admits two negative eigenvalues. Since it is symmetric, it has real eigenvalues. If λ_1, λ_2 and λ_3 are the eigenvalues and $\lambda_1 \geq \lambda_2 \geq \lambda_3$, the presence of the **vortex core requires that $\lambda_2 < 0$**.

This criterion is established in a general 3-D case. In the approximation of a 2D flow, it reads :

$$\nabla U = \begin{bmatrix} \frac{\partial u}{\partial x} & \frac{\partial u}{\partial y} & 0 \\ \frac{\partial v}{\partial x} & \frac{\partial v}{\partial y} & 0 \\ 0 & 0 & 0 \end{bmatrix} \quad \rightarrow \quad S = \tfrac{1}{2} * \begin{bmatrix} 2\frac{\partial u}{\partial x} & \frac{\partial u}{\partial y} + \frac{\partial v}{\partial x} & 0 \\ \frac{\partial u}{\partial y} + \frac{\partial v}{\partial x} & 2\frac{\partial v}{\partial y} & 0 \\ 0 & 0 & 0 \end{bmatrix} \quad and \quad \Omega = \tfrac{1}{2} * \begin{bmatrix} 0 & \frac{\partial u}{\partial y} - \frac{\partial v}{\partial x} & 0 \\ \frac{\partial v}{\partial x} - \frac{\partial u}{\partial y} & 0 & 0 \\ 0 & 0 & 0 \end{bmatrix}$$

then, using the continuity equation in 2-D incompressible flow, $\frac{\partial u}{\partial x} + \frac{\partial v}{\partial y} = 0$, we obtain the following tensor,

$$S^2+\Omega^2=\begin{bmatrix}\left(\frac{\partial u}{\partial x}\right)^2+\left(\frac{\partial u}{\partial y}*\frac{\partial v}{\partial x}\right) & 0 & 0\\ 0 & \left(\frac{\partial u}{\partial x}\right)^2+\left(\frac{\partial u}{\partial y}*\frac{\partial v}{\partial x}\right) & 0\\ 0 & 0 & 0\end{bmatrix}$$

This tensor presents a zero eigenvalue ($\lambda_1=0$) and a double eigenvalue ($\lambda_2=\lambda_3=\lambda$).

The new criterion becomes that in the core of a vortex, we have :

$$\lambda=\left(\frac{\partial u}{\partial x}\right)^2+\left(\frac{\partial u}{\partial y}*\frac{\partial v}{\partial x}\right)<0 \qquad (3.4)$$

Because of the particularity of the tensor of the velocity gradients, we have :

$$\lambda=\lambda_{S^2+\Omega^2}=\lambda_{S^2}+\lambda_{\Omega^2}$$

with $$\lambda_{S^2}=\left(\frac{\partial u}{\partial x}\right)^2+\frac{1}{4}\left(\frac{\partial u}{\partial y}+\frac{\partial v}{\partial x}\right)^2 \quad \text{and} \quad \lambda_{\Omega^2}=-\frac{1}{4}\left(\frac{\partial u}{\partial y}-\frac{\partial v}{\partial x}\right)^2$$

Thus $\lambda < 0$, the contribution of the rotation (λ_{Ω^2}) is superior to the contribution of the shear (λ_{S^2}). Supposing that the variation of u along x is small, we can schematize the signification of this criterion. As shown in fig 3.2, we see that λ is positive for a distortion (a), negative for a rotation (c), and zero for the intermediate case (b).

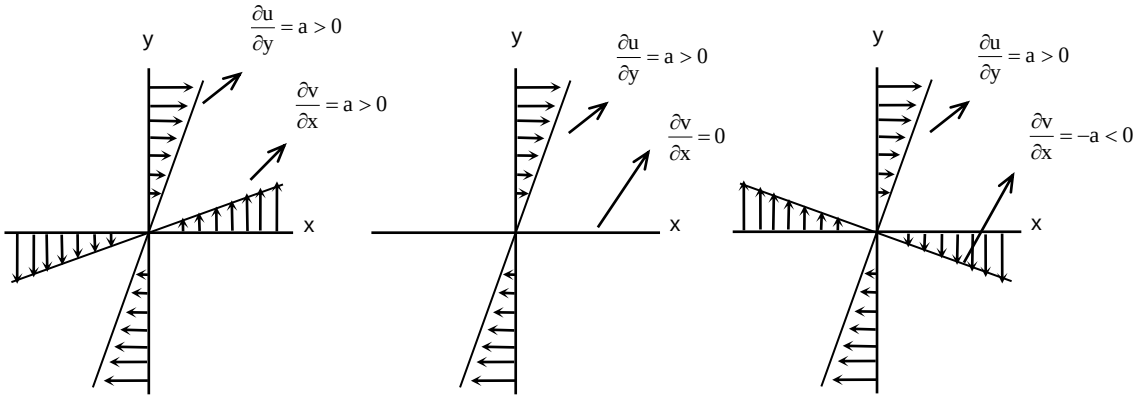

Figure 3.2 Sketches of the distortion and rotation

(a) pure distortion $\lambda > 0$ $(= a^2)$

(b) limit case $\lambda = 0$

(c) pure rotation $\lambda < 0$ $(= -a^2)$

Simply, $\lambda < 0$ means that within a vortex the derivatives of the velocity components must be of opposite signs. This exigency is not satisfied by the vorticity. For example, if they are of the same sign but if one is larger than the other, ω do not vanish even if the shear predominate. Finally, the eigenvalue λ is Galilean invariant as well as the vorticity because it is given only by derivatives of the velocity (Repellin (1999)).

3.4. Eduction of vortices by wavelet analysis

Once that a vortex has been defined and identified, one still has to find it in a flow field. This detection consists mainly in the determination of its position and of its size. From these two information, the other characteristics can be calculated. In order to make statistical averages on the vortices, this eduction should also be automatic.

In the present work, the eduction is done using the program initially developed at VKI by C. Schram and P. Rambaud, that uses the wavelet analysis on the vorticity field. The information about this program will be given in the next chapter which is called Post-Processing.

4 POST-PROCESSING OF THE PIV DATA

4.1 From the PIV pictures to the velocity fields

In each area of interest (downstream and upstream) a number of about one thousand PIV image couples has been acquired and post-processed with a home made cross-correlation algorithm, WIDIM (WIndow Displacement Iterative Multigrid) using Fast Fourier Transform algorithms. This program is based on an iterative multigrid predictor-corrector method, handling the window distortion (to better resolve the shear flows) and the sub-pixel window displacement (to limit the pixel-locking) (Scarano and Riethmuller (2000)). At the end of this PIV post-processing step a total of 1000 instantaneous velocity fields were obtained for each case.

The instantaneous velocity fields of N images obtained from W.I.D.I.M are processed to compute the mean velocity components and the turbulence intensities. Main velocity and turbulence intensities are defined as,

$$U_{mean} = \frac{1}{N}\sum_{i=1}^{N} U_i \tag{4.1}$$

$$\sqrt{\overline{u'^2}} = \sqrt{\left(\frac{1}{N}\sum_{i=1}^{N}\left(u_i - U_{mean}\right)^2\right)} \tag{4.2}$$

Similar expressions for V_{mean} and $\sqrt{\overline{v'^2}}$ can be written.

From this ensemble of instantaneous velocity fields, classical ensemble averages were computed and will be presented in the next section (i.e. maps of scaled mean velocity with streamlines, maps of scaled velocity fluctuation root mean square and maps of scaled Reynolds stress).

4.2 From the velocity fields to the vortex based statistics

In order to study a well-documented cavity dynamics from a vortex point of view, a homemade vortex recognition algorithm is used to extract conditional vorticity from the bank of instantaneous PIV velocity fields.

A brief but self contained description of this algorithm is given hereafter. A more detailed description can be found in Schram & Riethmuller (2001), and Schram et *al.* (2002).

From a given velocity field, the vorticity field is computed using a central and symmetrical four points stencil (3^{rd} order Richardson's finite difference scheme). The vorticity field is then squared to increase the "signal to noise ratio".

This map of positive values is analyzed in a continuous wavelet approach.

Wavelet analyze has been introduced in the turbulence field by Farge (1992). The wavelet based algorithm uses the right localization in the space and in the frequency domains of the analyzing wavelet family (Maar wavelet i.e. Mexican Hat wavelet). The choice of this mother wavelet has proved to be well adapted for vortex detection in the previous cited articles.

Each wavelet member (one by scale) of this analyzing family is passing on the square vorticity map signal and the resulting wavelet coefficients field is stored. From this 3D matrix, a search for local maximum wavelet coefficient is done over the field. At a given spatial location, a vortex is assigned if the corresponding wavelet coefficient is a local maximum over the scale. The core of the vortex is link to the scale (giving the maximum wavelet coefficient) by a calibration law obtain on an Oseen's type vortex (the core of Oseen vortex is defined as the diameter of the region for which the tangential velocity is linearly increasing).

These different tests would be inefficient without the use of user-defined thresholds. In this perspective, before the validation of the presence of a vortex like structure two tests have to be satisfied. The first one check locally (at the position of the candidate vortex) that the flow is mainly rotating by using the λ_2 criteria introduced by Jeong & Hussain (1995) (λ_2 second eigenvalue of the tensor gradient of velocity). The 2D version of this criterion is used here with success to filter out the pure shear of the shear-layer. In the second test, the selected wavelet coefficient is compared to the

wavelet coefficient of an Oseen vortex (of the same size). This comparison leads to a successful test if the resemblance with an Oseen's type vortex is superior to 50%.

In the present application, the threshold related to λ_2 has been fixed to four times the standard deviation of λ_2 (taking into account only the negative part). This empirical value has been visually found to be high enough to filter out the shear layer like events but not too high to still capture the vortex like events.

If those two tests are validated then the candidate vortex is allowed to enter in the vortex database.

4.3 A practical example of vortex detection

In this paragraph, a vortex identification on an instantaneous flow field is shown step by step through an example.

In Figure 4.1, an intantaneous velocity vector field obtained from PIV measurements is presented (upstream configuration).

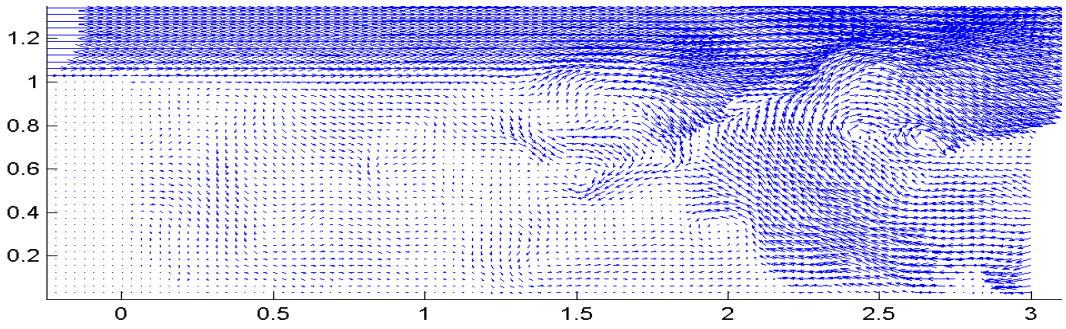

Figure 4.1 Instantaneous vectors flow field.

This field of view includes several vorticity patches as shown in Figure 4.2.

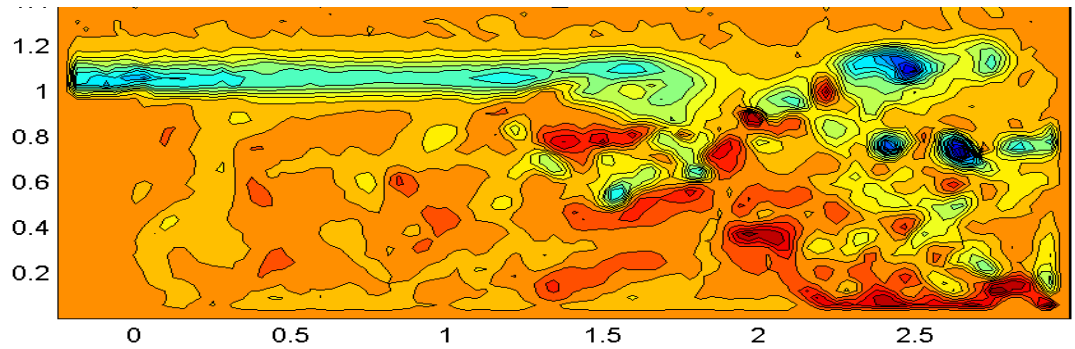

Figure 4.2 Instantaneous vorticity field.

At this point, it is important to remind that although a vortex presents always a peak of vorticity, a peak of vorticity is not always a vortex. In particular, the presence of a detached shear layer is clearly noticeable. The figure 4.3 shows that λ_2 will clearly filtered out the non purely rotating part of this vorticity.

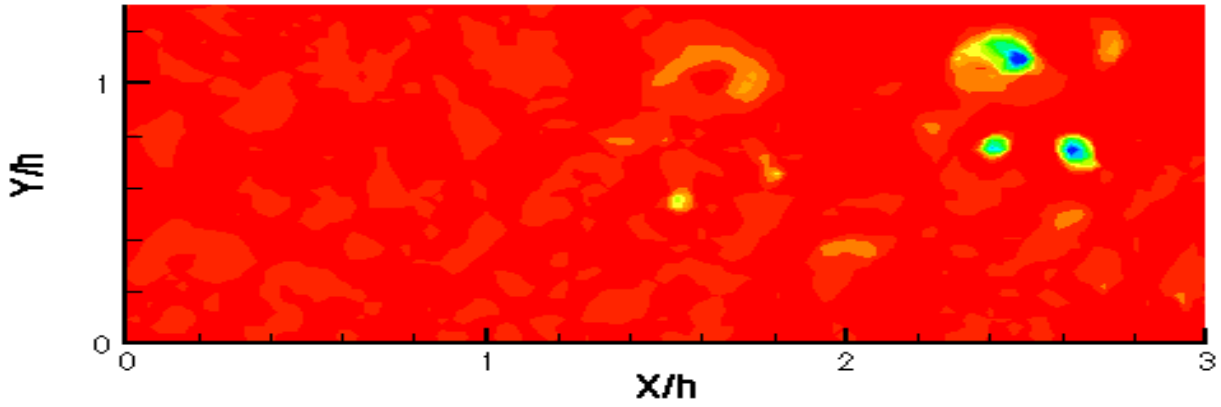

Figure 4.3 Instantaneous negative lambda field

Finally, Figure 4.4 presents the location of three candidates vortex kept by the wavelet algorithm associated with the flow field displayed in Figure 4.1.

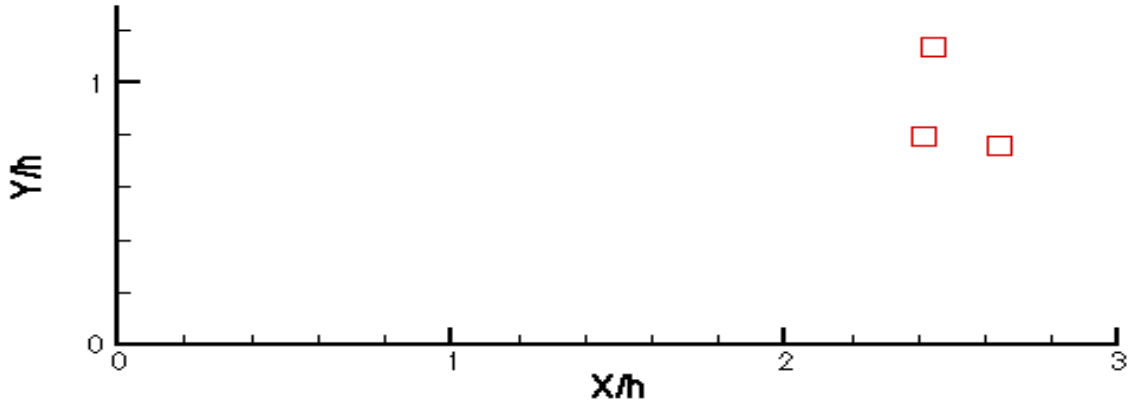

Figure 4.4 Instantaneous vortex locations by wavelet analysis

5 RESULTS AND DISCUSSION

This section contains the analysis of cavity flow and vortex dynamics by looking into its flow dynamics. For clarity, the following results can be thought into two main categories. The first one is concerned with the mean velocity modulus, standard deviation of the velocity and Reynolds shear stress results coming from WIDIM post-processing. The second part focuses on the results from the vortex database. In both part, the results are non-dimensionalized.

5.1. Velocity Distribution

The velocity modulus distribution and the streamlines of the cavity flows under an increasing Reynolds number are presented in Fig.5.1.In this figure, the color map is attached to the modulus of velocity.

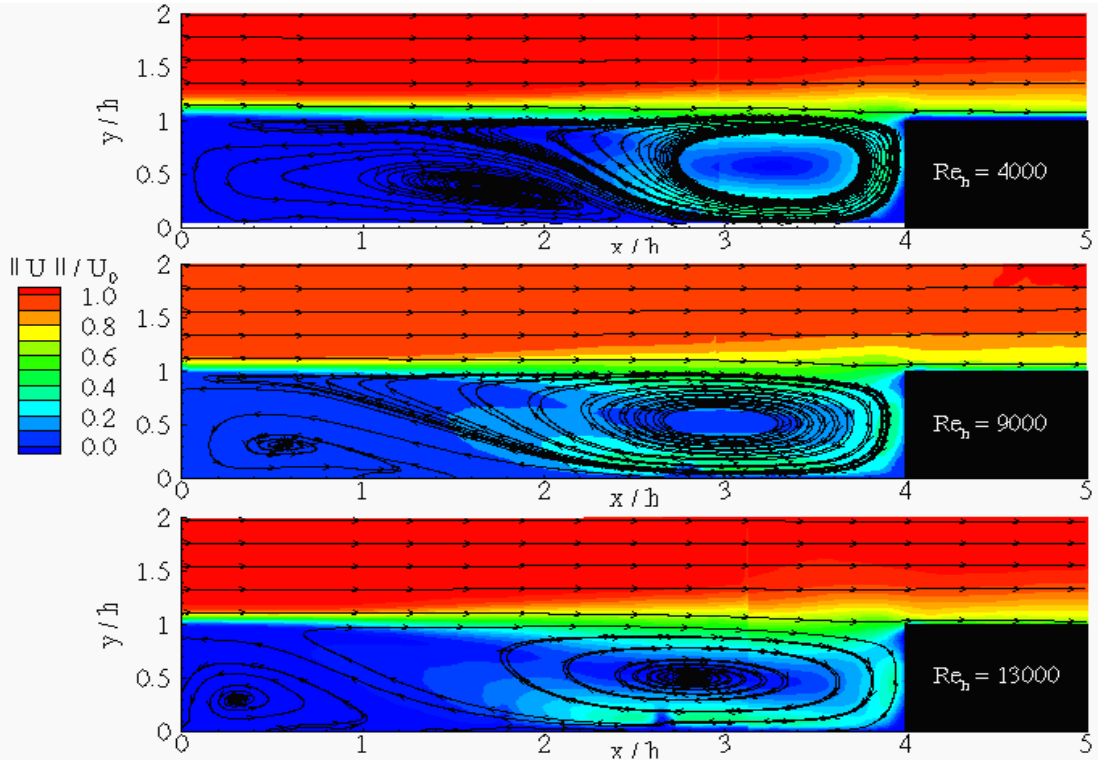

Figure 5.1: Map of velocity modulus and streamlines for an increasing Reynolds number

The common features of the examined flows are the presence of two main recirculation bubbles filling the whole cavity. The first bubble (upstream) is turning in anti-clockwise sense whereas the second bubble (downstream) is turning in clockwise sense. Following the cavity designations reviewed by Komerath et al. (1987), the cavity flow under investigation is a shallow one (L/h>1). With the same designations Figure 5.1 shows also that the cavity is an open type cavity (there is no streamline connecting directly to the bottom of the cavity).

It is observed that the centers of the first and second recirculation bubbles are moving in the upstream direction when the Reynolds number increases. This phenomenon is thought to be due to the stronger energy given by the free stream flow to the clockwise recirculation bubble. Same behaviour was observed by Ghia et al. (1982) (in Shankar and Despande 2000) for a square lid drriven cavity for the Reynolds number between 100 to 10000. It may be roughly estimated that this clockwise recirculation bubble occupies 60% (Re = 4000), 72% (Re = 9000) & 82% (Re = 13000) of the whole cavity surface and the de-attachment point on the bottom of the cavity separating the two bubbles are located in the interval [2.5h;3.0h](Re = 4000), [2.0h;2.5h](Re = 9000) & [1.5h;2.0h](Re = 13000).

5.2 Turbulence Intensities

In Figure 5.2 RMS values of u velocity component are presented. This figure indicates that the increase in flow speed over the cavity has an important impact on the turbulent character of the flow

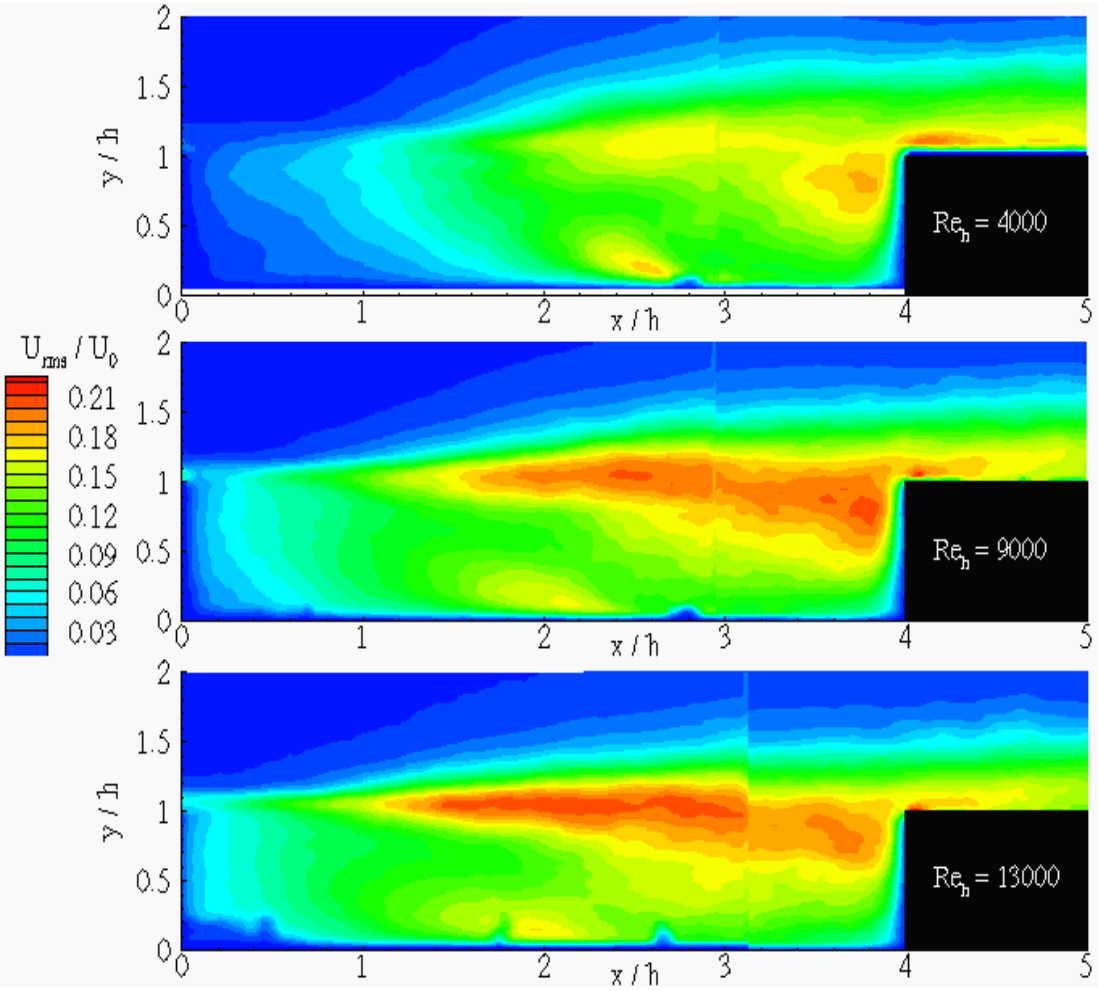

Figure 5.2: Map of u_{rms} for an increasing Reynolds number

In the case of low speed (ie., Re=4000) the high Urms regions appear only near the upstream of the rear wall and elsewhere the stream wise turbulence is more or less low and homogeneous. When the inflow speed increases, the turbulence augments about the shear layer. Finally when the Reynolds number is 13000, the interface between the free stream and the cavity flow is flooded by high levels of Urms. The maximum value for this rms velocity scaled by the free stream velocity is about 20% for the higher Reynolds number (Re=13000).

Nevertheless, it has been noticed that the scaled rms associated with the *v* component (Figure 5.3), is decreasing when the Reynolds number increases from 4000 to 13000.

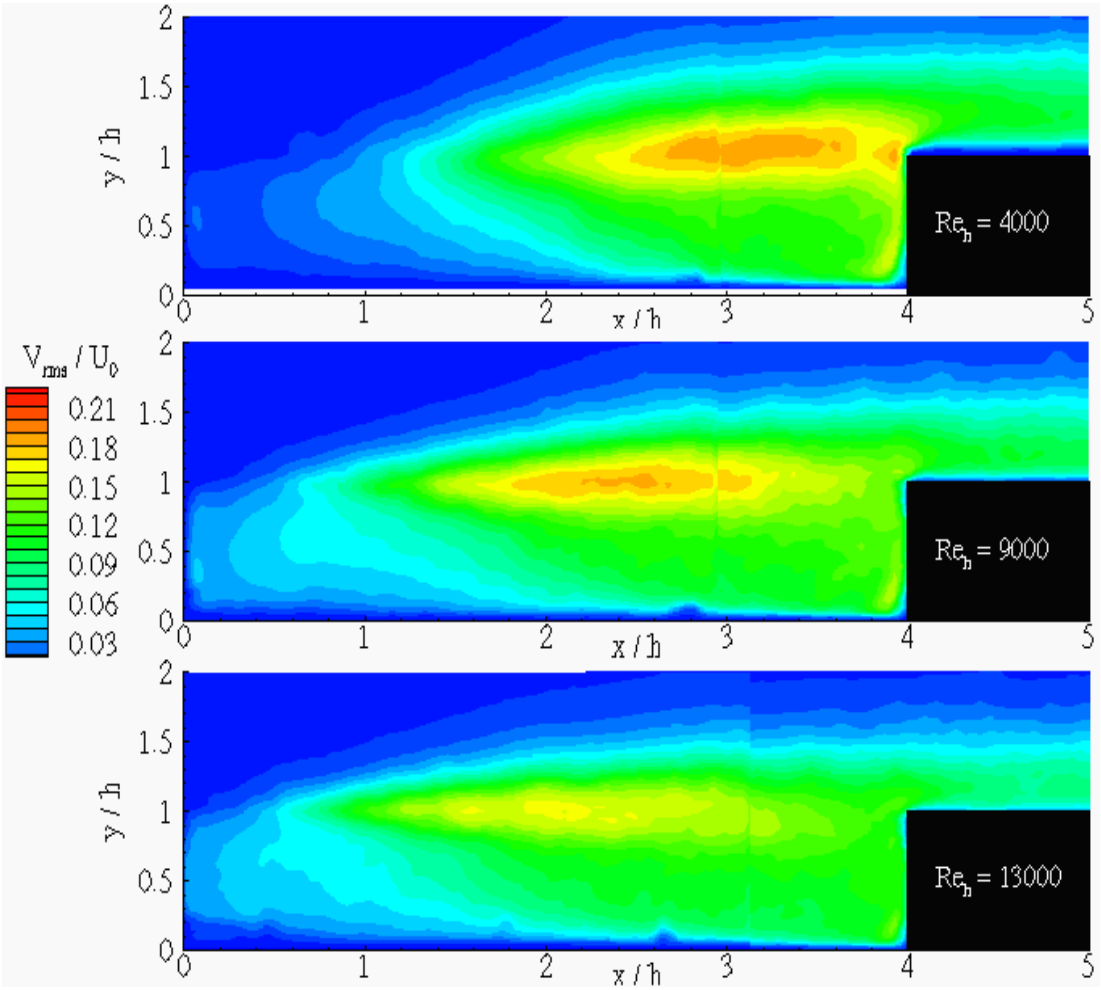

Figure 5.3: Map of v_{rms} for an increasing Reynolds number

This phenomenon, already underlined by Karamcheti (1955) and Komerath et al. (1987), is due to the Kelvin-Helmholtz instabilities. Instabilities introduce to the shear layer strong periodical oscillations when the flow outside the cavity is laminar (with a turbulent flow outside the cavity those shear-layer oscillations had been observed to be less significant Karamcheti (1955)).

5.3 Reynolds Stress

In Figure 5.4, the Reynolds shear stress distribution non-dimensionalized by the square of the free stream velocity is shown.

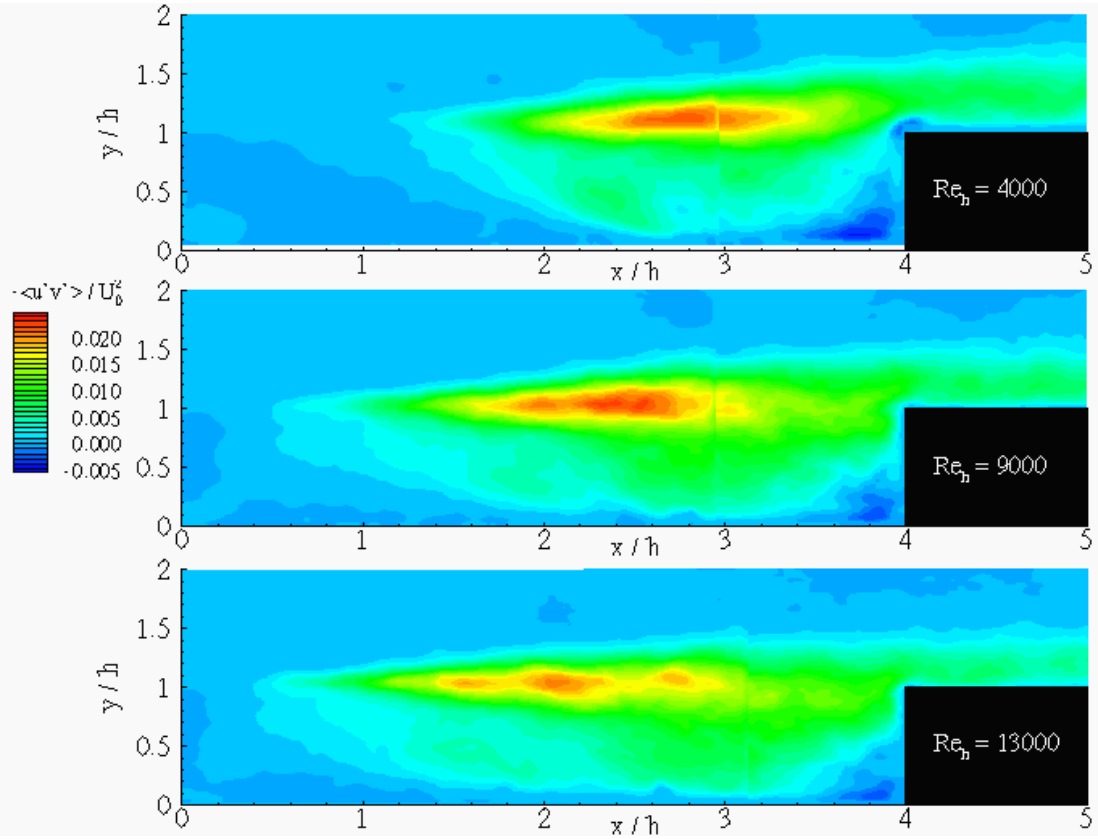

Figure5.4: Map of Reynolds stress for an increasing Reynolds number

It is found that the Reynolds number has a weak influence on the maximum value of this variable. Nevertheless, it is observed that the location of the maximum shear stress is moving towards the leading edge (as it was the case for the center of the cavity recirculation bubbles).

In Figure 5.5, the variation of the non-dimensional Reynolds stresses along the length of the cavity (non-dimensionalized by the momentum thicknes of the inflow boundary layer) on the line y/h = 1 is presented in a logarithmic scale. It is found that this figure agrees well with the results of Gharib and Roshko (1987). In this last reference, the authors were using an axis-symmetrical cavity operated with water under three different Reynolds number values (based on the free stream velocity and

the momentum thickness). They found out that the maximum Reynolds shear stress was exponentially growing till a region of saturation then it was decreasing before the trailing edge.

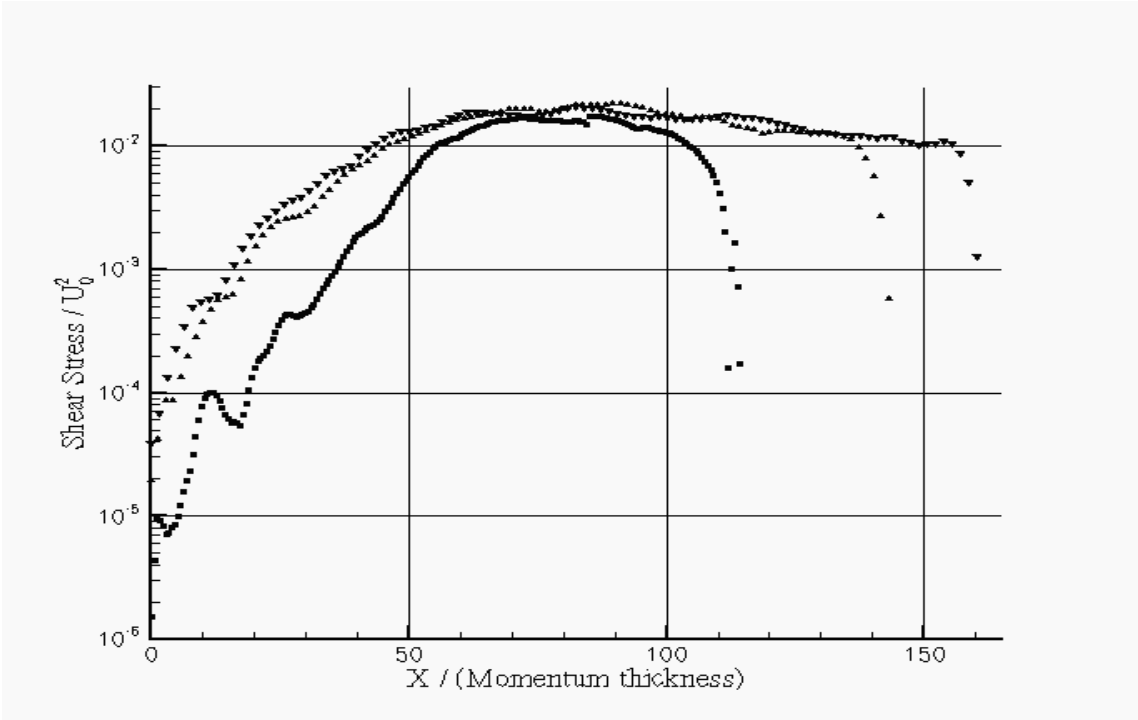

Figure 5.5: Growth of the maximum reynolds stress (at y/h = 1.) in the cavity shear layer versus downstream distance scaled by momentum thickness (■ for Re = 4000,▲ for Re = 9000,▼ for Re = 13000)

In the present work similar behavior is found with a slight difference. In their experiments Gharib and Roshko (1987) were working in the range of $Re_\theta \in [85;130]$ in comparison of $Re_\theta \in [160;366]$ in the present work, in the Figure 5.5, the squared symbols represent the variation of the maximum shear stress along the cavity entry for $Re_\theta=160$. This grow is following an exponential law (the slope is linear in semi-log), in a case associated with the highest oscillation of the shear layer. For the two others Reynolds number ($Re_\theta=260$ & 366), the slope is closer to a linear law characterizing a less strong oscillation of the shear layer. It is a confirmation that the shear layer is oscillating more when the free stream flow is more laminar (i.e. Karamcheti (1955)). Finally, let's remind the experiment on axial cavity of Sarohia (1977) at $Re_\theta=242$, where the growth of the shear layer was found almost linear which is corresponding to the range of Re_θ for which a linear growth of the maximum Reynolds shear stress is found.

5.4. Distribution of the Detected Vortices:

In Figure 5.6, a view of the vortices detected from the PIV measurements by using the wavelet analyses are presented.

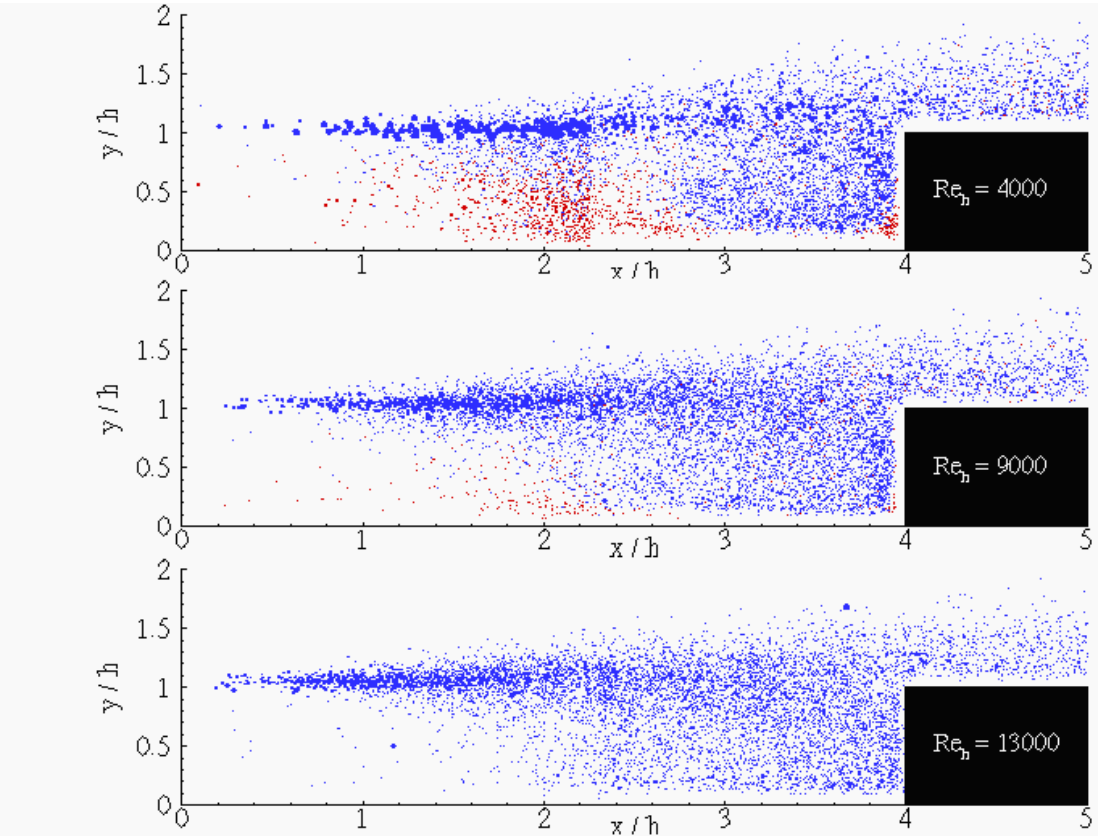

Figure 5.6: Map of vortex location for an increasing Reynolds number

For clarity, the vortex cores are not shown in their real size spanning between 0.12h - 0.54h. However, it is noticeable that the size of the bigger vortices embedded in the shear layer is decreasing with the Reynolds number. This conclusion can be considered as a result of the change in the boundary layer thickness with varying Reynolds numbers.

In all the three cases, the pattern drawn by the vortices looks like a “jet flow” attached to the leading edge.

In order to give detailed information about the common vortex behavior, only one case (for Re=4000) is taken and shown in Figure 5.7. This figure presents all the positions and sizes of the vortices extracted and collected in the vortex database.

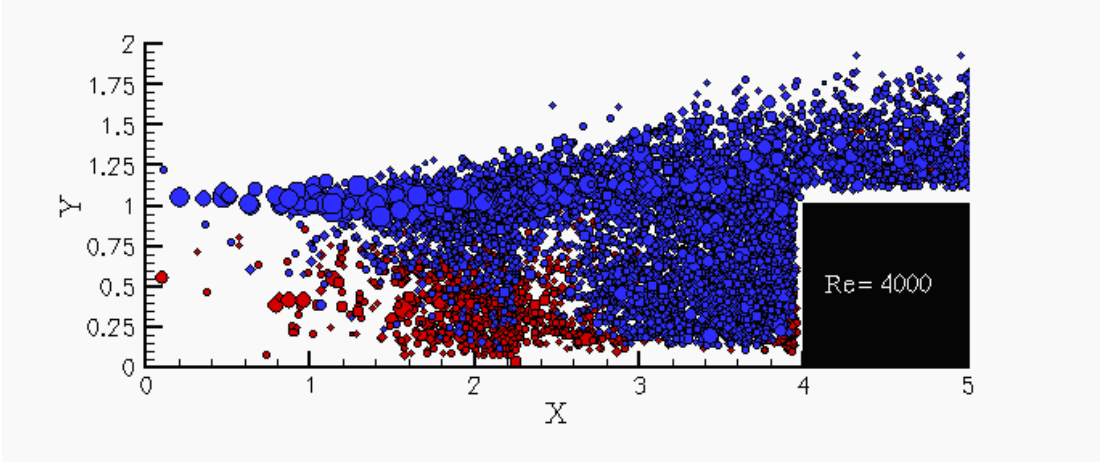

Figure 5.7: Map of vortex location for Re=4000

The “blue” symbols are associated with clockwise vortices and the “red” ones are anti-clockwise vortices. It appears that the “blue” vortices seem to be created in the shear layer close to the leading edge. Those vortices are then convected in the downstream direction with the possibility to enter in the cavity or to pass over (impinge) the trailing edge. The blue vortices inside of the cavity are mainly located in the clockwise recirculation bubble. In the lower Reynolds number case associated with the higher fluctuation of the shear layer and the bigger vortices imbedded inside the same shear layer, it is found that a bigger amount of “red” vortices is present. Those vortices seem to be created along the trailing wall, especially close to the bottom of the cavity (higher concentration of “red” vortices in the right corner of the cavity in the figure 5.6 for Re = 4000). Those second type of vortices seem to be driven by the clockwise recirculation bubble towards the region inside of the cavity separating the two bubbles. Afterward, those “red” vortices seem to be trapped mainly in the anti-clockwise recirculation bubble.

When the Reynolds number increase the occurrence of big “blue” vortices seems to decrease as well as v_{rms} at the “mouth” of the cavity, as a consequence the presence of red vortices is strongly reduced. (Figure 5.6)

5.5. Relation between vortex size and their circulation.

The Figure 5.8 shows the core size of extracted vortex versus their dimensionless circulation.

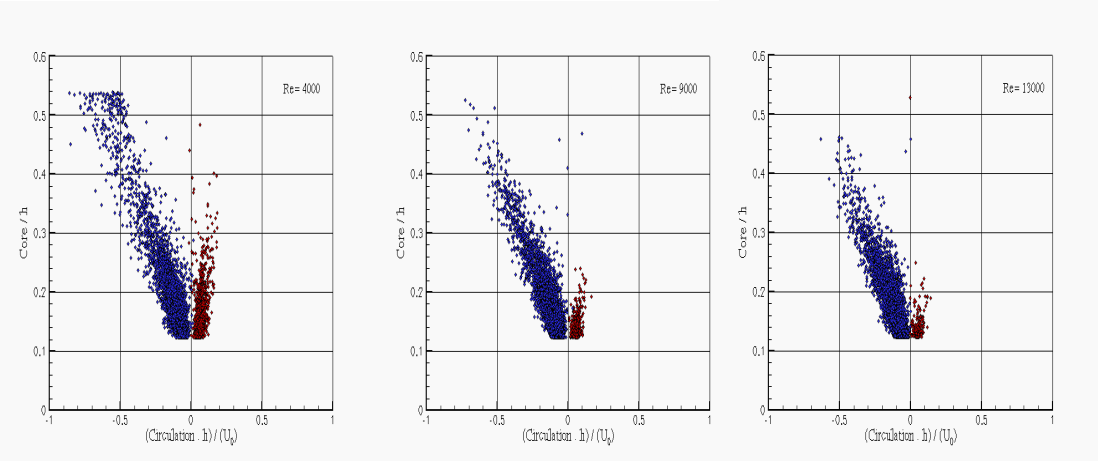

Figure 5.8: Dimensionless core size versus dimensionless circulation for the cavity at (Re =4000, 9000, 13000)

This last variable is found by summation of the vorticity on a surface limited by the core diameter. It can be observed that the slope is different depending of the sign of the circulation that is probably due to the level of the vorticity and the size of the shear layer creating those vortices. The minimum and maximum sizes researched inside of the flows where fixed in the range [0.12h;0.54h]. In the lower Reynolds number the maximum core size seems to be cut (Reynolds = 4000) and the flow is probably containing bigger events. This maximum core size was high enough to catch all the events associated with the Reynolds 9000 and 13000. It is clear that the smaller scales are also probably present in the cavity but they were not taken (for an evident resolution point of view). For Reynolds number equals to 13000, it appears that a small number of “red” vortices are indeed extracted.

6 CONCLUSIONS

In the present thesis, vortex behavior (in terms of vortex size, energy content, and their pattern in the cavity.) in a low speed cavity flow is investigated for three different Reynolds numbers. (Re=4000, 9000, 13000).

The experimental part of this study was carried out by particle image velocimetry (PIV). Experiments were made on rectangular cavities and the cavity length to depth ratio (L/d=4) was kept constant during measurements. The regime of the upstream boundary layer was also investigated by hot wire measurements and found in laminar case. An extensive amount of instantaneous velocity fields are taken from PIV measurements and processed to obtain the major vortices by using wavelet analysis. Those vortices are reported in the literature survey as a key point feature.

In all cases, cavity flows were belonging to an open type and were mainly characterized by two large circulating bubbles turning in different directions. As the Reynolds number increased, the downstream recirculation bubble becomes larger and its center moves through the leading edge. Consequently the upstream recirculation decreases in size. The enlargement of the downstream recirculation bubble with increasing free stream velocity was attributed to the increasing energizing effect of the shear layer.

The sensibility to the Reynolds number is observed through an increase of the scaled stream wise velocity standard deviation (with a top value around of 20%) when the Reynolds number is increasing. For the scaled standard deviation associated with the V component, an opposite tendency is observed as previously reported in the literature.

The Reynolds number has been found to have a weak influence on the maximum value of the scaled Reynolds shear stress. However, it is found that the location of the maximum Reynolds shear stress is moving towards the leading edge and its growth on the mouth of the cavity is Reynolds number dependent. In the lower

Reynolds number case this growth is found exponential and linear for the other two cases. This growth has been reported also in previous works.

The novelty of the present work consists in the vortex-based statistics. An overview of the position occupied by the vortices was found similar to a jet attached to the leading edge. Two main area of vortex production were identified. Clockwise vortices are created inside of the shear layer, convected appearing with a higher probability inside of the trailing recirculation bubble. Anti-clockwise vortices were mainly created by the trailing wall-layer. Their concentration at lower Reynolds number seems to be higher in the leading edge recirculation bubble.

It is observed that the size of the vortices is link to the size of the incoming boundary layer and this size decrease when the Reynolds number increases.

It is hoped that the present thesis makes invaluable contribution for the further studies in the same filed.

REFERENCES

Farge M. (1992) “Wavelet transforms and their applications to turbulence”. Ann. Rev. Fluid Mech. 24: 395-457.

Gharib M., Roshko A. (1987) “The effect of flow oscillations on cavity drag”, J. Fluid Mech., vol. 177, pp. 501-530.

Jeong J., Hussain F. (1995) “On the identification of a vortex”, J. Fluid Mech. Vol. 285: 69-94.

Karamcheti K. (1955) “Sound Radiation from rectangular cutouts” NACA TN 3488, August.

Komerath N.M., Ahuja K.K., Chambers F.W. (1987) “Prediction and measurement of flows over cavities. A survey.” IAAA

Raffel M.; Willert C.; Kompenhans J. (1998) Particle Image Velocimetry – Practical Guide (Ed. Springer, Berlin)

Repellin O. (1998). “ Experimental Characterization of Vortical Structures with Aeroacoustic Effects”, VKI Project Report, Von Karman Institute, June 1999

Rockwell D.; Naudascher E. (1978) “Review-Self Sustaining Oscillations of Flow Past cavities” Journal of Fluids Engineering, Vol.100

Rossiter J E. (1964) “Wind tunnel Experiments on the Flow over Rectangular Cavities at Subsonic and Transonic Speeds” Royal Aircraft Establishment Technical Report No.64037

Sarohia V. (1977) “Experimental investigation of oscillations in flows over shallow cavities” AIAA Journal Vol. 15, No. 7.

Scarano F.; Riethmuller M.L. (2000) Advances in iterative multigrid PIV image processing. Exp Fluids 29: S51-S60.

Scarano F. (2002) Iterative image deformation methods in PIV. Meas. Sci. Tech. 13: R1-R19.

Schlichting H. (1968). Boundary Layer Theory, Six edition, Mc Graw-Hill Book Company. pp:129

Schram C.; Riethmuller M.L. (2001) Vortex ring evolution in an impulsively started jet using digital particle velocimetry and continuous wavelet analysis. Meas. Sci. Tech. 12: 1413-1421.

Schram C.; Rambaud P.; M.L. Riethmuller (2003) Wavelet based coherent structure eduction from a backward facing step flow investigated using particle image velocimetry. (To be published)

Shankar P. N. and Deshpande M. D. (2000) “Fluid mechanics in the driven cavity” Annu. Rev. Fluid Mech. 32: 93-136.

Tam C.K.W., P.J.W. Block (1978) “On the tones and pressure oscillations induced by flow over rectangular cavities”, J. Fluid Mech., vol. 89, part 2, pp. 373-399.

White M Frank. (1991). Viscous Fluid Flows, Second edition, Mc Graw-Hill, Inc. pp:222,223

RESUME

Elif Özsoy was born in Ankara in 1976. She received her B.Sc. degrees in Aerospace Engineering in 1999 as a second one and Aeronautics Engineering in 2000 from Istanbul Technical University, Faculty of Aeronautics and Astronautics.

Between 2001-2002 , she attended von Karman Institute for Fluid Dynamics "Diploma Course Program" .

Since September 2000, she has been a student of M.Sc program of Institute of Science and Technology in the Aeronautics Engineering Department.